

RESEARCH ARTICLE

10.1029/2018JB015938

Key Points:

- A 3-D crustal shear-wave velocity model of Taiwan Strait and Fujian, SE China, was obtained from ambient noise tomography
- Geological units were influenced by older to younger tectonic events from northwest to southeast in the study region
- Two-stage extension with different centers occurring in the early and late Cenozoic may account for the structural pattern in the strait

Supporting Information:

- Supporting Information S1

Correspondence to:

H. Yao,
hjyao@ustc.edu.cn

Citation:

Zhang, Y., Yao, H., Yang, H.-Y., Cai, H.-T., Fang, H., Xu, J., et al. (2018). 3-D crustal shear-wave velocity structure of the Taiwan Strait and Fujian, SE China, revealed by ambient noise tomography. *Journal of Geophysical Research: Solid Earth*, 123. <https://doi.org/10.1029/2018JB015938>

Received 10 APR 2018

Accepted 4 SEP 2018

Accepted article online 6 SEP 2018

3-D Crustal Shear-Wave Velocity Structure of the Taiwan Strait and Fujian, SE China, Revealed by Ambient Noise Tomography

Yayun Zhang¹, Huajian Yao¹ , Hsin-Ying Yang¹, Hui-Teng Cai², Hongjian Fang¹ , Jiajun Xu^{1,2}, Xing Jin², Hao Kuo-Chen³ , Wen-Tzong Liang⁴ , and Kai-Xun Chen^{3,5} 

¹Laboratory of Seismology and Physics of Earth's Interior, School of Earth and Space Sciences, University of Science and Technology of China, Hefei, China, ²Earthquake Administration of Fujian Province, Fuzhou, China, ³Department of Earth Sciences, National Central University, Taoyuan, Taiwan, ⁴Academia Sinica, Institute of Earth Sciences, Taipei, Taiwan, ⁵Department of Geosciences, National Taiwan University, Taipei, Taiwan

Abstract The Taiwan Strait, along with the southeastern continental margin of the Eurasian plate, Fujian in SE China, is not far from the convergent boundary between the Eurasian plate and the Philippine Sea plate. Although this region is considered tectonically relatively inactive, many small earthquakes still occur, and normal faults are well developed in the strait. To better understand the geological processes in this region, we use 2 years of ambient noise data from more than 100 stations in Fujian and Taiwan to obtain a 3-D crustal shear-wave velocity model using a direct surface-wave inversion method. Our results show that the low-velocity zone beneath the Zhenghe-Dapu suture zone plays an important role in the tectonic evolution of the Fujian area. The relatively high velocity in the eastern part of the suture zone and low velocity in the west correspond to the Mesozoic magmatic zone and the Wuyi-Yunkai orogenic belt in Fujian, respectively. The coastline of Fujian presents a high-velocity anomaly in the upper crust, which is related to the Mesozoic Pingtan-Dongshan metamorphic belt. The long strip-like high-velocity zone through the rift basins in the strait is interpreted as igneous rocks due to extension of the lithosphere in the Cenozoic. Two-stage extension with different extensive centers in the strait may be the reason for the high- and low-velocity anomalies in the middle to lower crust and uppermost mantle of the strait.

1. Introduction

The southeastern margin of China is located in the oblique convergence zone of the Eurasian (ES) plate and the Philippine Sea (PHS) plate, which is a typical model in a trench-arc-basin system (Figure 1). Previous studies have shown that the two plates converge at a rate of approximately 80 mm/year in the direction of N53°W, with the PHS plate subducting northward under the ES Plate along the Ryukyu trench, while to the south of Taiwan, the ES margin underlies the PHS plate eastward along the Manila subduction zone (Seno & Kawanishi, 2009; Yu et al., 1997; H. W. Zheng et al., 2013). Due to the complex tectonic evolution and the orogenesis in Taiwan, Taiwan Island and its southern and eastern offshore areas have always been a region of interest for studying the collision process between the continental plate and oceanic slab.

Compared to the active convergent region, the Taiwan Strait appears much quieter because it is relatively stable in terms of seismicity distribution (Figure 1a). Based on the distribution of normal faults in the strait (Gao & Huang, 1995), this region can be simply divided into three parts from south to north: Tainan Basin (TNB), Penghu-Beigang Uplift, and many extensional basins in the middle and north parts (Figure 1a). The strait has shallow water depths (less than 100 m), fewer structurally active zones, and fewer earthquakes. However, it is important to study the collision process and structural development of the whole region, especially during the Cenozoic. The rifting in the early Cenozoic with lithospheric extension, which led to the formation of the fault-bounded basins in the north and middle parts of the strait, had a marked impact on the architecture and stratigraphy of the strait following crustal uplift and continental breakup (A. T. Lin et al., 2003). After this stage, the strait entered a postrift period from the Oligocene initiation of seafloor spreading in the South China Sea to the Miocene, which mainly influenced the strata of the southern part of the strait, such as the formation and thickness of the sediments in TNB. The area transferred to foreland basin development in the late Cenozoic because of the termination of the extension caused by arc-continental collision.

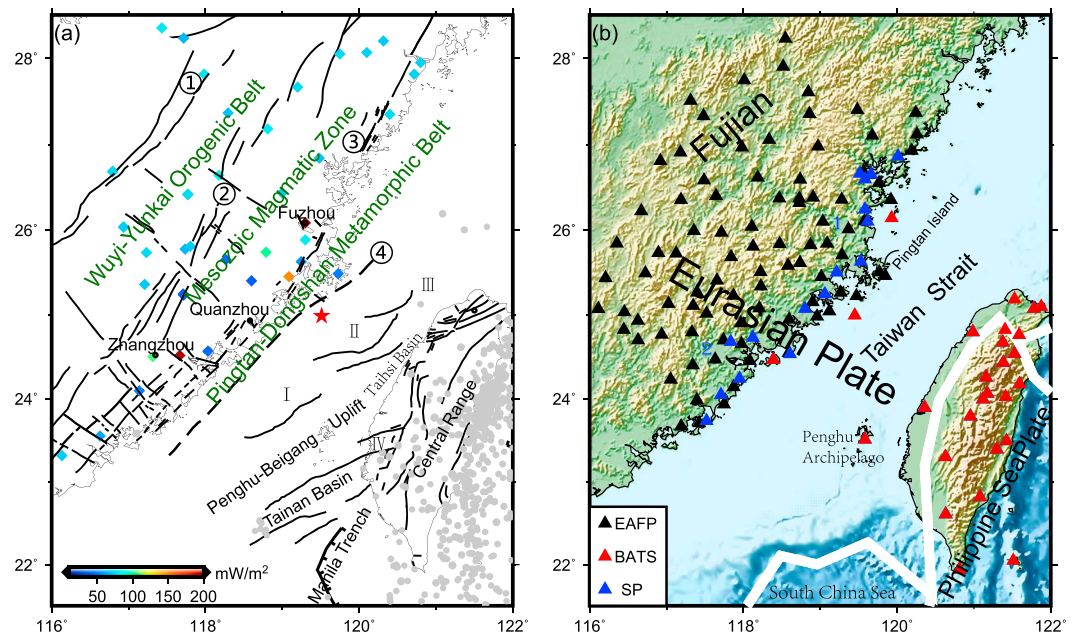


Figure 1. (a) Tectonic setting of the study region. (Colored diamonds) Heat flow measurements (Hu et al., 2000; Y. Wang, 2001) with values indicated by the color bar. (Red star) Epicenter of the 1604 magnitude 8 earthquake. (Gray dots) Earthquakes from 1918 to 2018 with the magnitudes ≥ 5 downloaded from the U.S. Geological Survey. The solid black lines denote faults, and the dashed line (④) represents the Fujian littoral fault with uncertainty (the position of Fujian littoral fault is still controversial). The three NE-SW-trending suture zones in Fujian: ① Shaowu-Heyuan fault zone; ② Zhenghe-Dapu fault zone; ③ Changle-Zhaoan fault zone. I = Penghu Basin; II = Nanjihtao Basin; III = Kuanyin platform; IV = Peikang High. (b) Topography of the study region and the distribution of the stations (colored triangles). Different colors denote different seismic networks. (White wide lines) Plate boundaries from Bird (2003). 1 = Fuzhou Basin; 2 = Zhangzhou Basin. EAFP = Earthquake Administration of Fujian Province; BATS = Broadband Array in Taiwan for Seismology; SP = SinoProbe Project.

Early studies mainly focused on the formation and development of the shallow crustal structure and sedimentary basins on a local scale (A. T. Lin & Watts, 2002; A. T. Lin et al., 2003).

The Moho depth has been relatively well resolved in this region. Receiver functions (Ai et al., 2007; He et al., 2014), gravity data (Hsieh et al., 2010), and tomography with body waves (Kuo et al., 2015) and surface waves (K. X. Chen et al., 2016; Y. C. Huang, Yao, et al., 2014) have all been used to determine the Moho depth. The results have generally agreed that the Moho depth in the strait is shallower than 30 km. The Fujian area has a relatively thicker crust with a depth of more than 30 km. However, this interface in Taiwan Island appears very complicated, and most parts of western and middle Taiwan have a much deeper Moho interface due to the orogeny in the late Cenozoic. However, the easternmost part of the island has very thin oceanic crust. In addition, K. X. Chen et al. (2016) used ambient noise tomography to invert for the shear-wave velocity structure of the crust and uppermost mantle of the strait and Taiwan Island and indicated there may have been a cooling magma reservoir and feeding system in the deep crust and upper mantle beneath Penghu Island.

To the northwest of the strait, the Fujian area, as the continental margin of southeastern Asia, has undergone a series of tectonic episodes since the Neoproterozoic (Shu et al., 2011), which led the continental block to split into many small blocks forming uplifts and depressions bounded by NE-SW- and NW-SE-oriented faults. The subduction of the paleo-Pacific plate in the late Mesozoic led to the wide distribution of igneous rocks in this area (Zhou et al., 2006), which may account for the high heat flow along the coastal region of Fujian (Hu et al., 2000; Y. Wang, 2001; Figure 1a). In the Cenozoic, the convergence between the ES and PHS plates and the opening of South China Sea played important roles in reconstructing the Fujian area. The complicated tectonics has been reflected in the petrology and geomorphology. The main pattern of fault distribution in Fujian exhibits a crossed-grid style (P. Z. Wang et al., 1993; Figure 1a). Three major faults in this continental area trend NNE-NE, namely, the Shaowu-Heyuan fault zone, Zhenghe-Dapu (ZH-DP) fault zone, and Changle-Zhaoan (CL-ZA) fault zone (Figure 1a). The ZH-DP fault (or suture) zone separates the Cretaceous

magmatic downfaulted belt to the east and the Wuyi-Yunkai fold belt to the west; the CL-ZA fault zone lies almost along the coast and demarcates the eastern boundary of the magmatic zone and the western boundary of a Mesozoic metamorphic zone (W. S. Chen et al., 2002) named the Pingtan-Dongshan metamorphic belt (PDMB; Figure 1a). The belt is bounded by an offshore NNE-oriented fault, the Fujian littoral fault (FLF; Figure 1a) to the east. The FLF is an important and active fault belt that controls the tectonic activity as well as the formation and evolution of the western strait (Zhan et al., 2004). The belt has experienced several stages of tectonic movement since the late Mesozoic and extended as far as the northwest South China Sea. This region is also characterized by many small NNW- to NW-oriented faults perpendicular to the main faults, which is not found in Taiwan where NE-trending tectonic units are dominant (Kuo-Chen, Wu, & Roecker, 2012). The seismicity in this region coincides highly with the intersection of the two fault systems (NNE- or NE- and NW-trending faults), such as in the Fuzhou and Zhangzhou downfaulted basins and the Quanzhou Gulf. Most earthquakes occur in the crust with magnitudes less than M_s 5 (Cai et al., 2015). In 1604, an intensely destructive earthquake with a magnitude of approximately 8 occurred in the offshore area of Quanzhou, which was the largest earthquake in historical records in this area. Efforts have been made to investigate small-scale structures beneath Fujian and adjacent regions; for example, several 2-D profiles have been produced with deep seismic sounding (Cai et al., 2016; Kuo et al., 2015; P. Li et al., 2015). In addition, a well-resolved 3-D P wave velocity model of this area using body-wave traveltimes from active sources and earthquakes (Cai et al., 2015) has been completed.

Although many studies have been performed in southeastern China, many problems remain unsolved because of the obscure and complicated structural deformation during the complex tectonic history. Located just west of the collision zone, the Taiwan Strait and Fujian area play important roles in the regional tectonic and dynamic evolution history of SE China. However, the influences of different tectonic processes such as the subduction of the paleo-Pacific plate, the opening of the South China Sea, and the ongoing convergence on this region are still poorly understood. The locations of small faults in this area, the dynamic processes, and even the eastern termination of the subducted ES plate, however, have long been controversial. These questions require a more accurate 3-D velocity model of the crust and upper mantle from Taiwan to Fujian encompassing the strait area. Previous studies, however, have always concentrated on large-scale structures in southeastern Asia and interface information mainly in the crustal range using body waves.

In this study, we use ambient noise data from more than 100 stations deployed in this region to extract Rayleigh wave dispersion. Since surface waves at shorter periods are more sensitive to shallower structures, we obtain a more detailed shear-wave velocity model of this region after applying a direct surface-wave tomography method based on period-dependent ray-tracing. Finally, we discuss the geological and tectonic implications of the tomographic results in Fujian and the Taiwan Strait.

2. Data and Methods

2.1. Station Distribution and Ambient Noise Analysis

Due to the yearly increase in the number of digital seismic stations across the strait, the resolution of tomography can be much improved. In this study, we utilize 2 years (2014–2015) of continuous seismic records from 88 permanent stations in the seismic network of the Earthquake Administration of Fujian Province (Data Management Centre of China National Seismic Network, 2007; X. F. Zheng et al., 2010) and 25 stations of the Broadband Array in Taiwan for Seismology (Institute of Earth Sciences, Academia Sinica, Taiwan, 1996) (Figure 1b). In addition, a few hundred phase-velocity dispersion curves by K. X. Chen et al. (2016) extracted from 23 stations from the Broadband Array in Taiwan for Seismology, 6 stations from the Earthquake Administration of Fujian Province, and 16 SinoProbe stations are included to produce more accurate results.

It has been well known that continuous ambient seismic noise cross-correlation between two stations can be used to retrieve empirical Green's functions (F. C. Lin et al., 2008; Shapiro & Campillo, 2004; Y. Yang et al., 2007; Yao et al., 2006). Surface-wave dispersion data extracted from empirical Green's functions can be further inverted for shear-wave velocity structures of the crust and upper mantle (e.g., K. X. Chen et al., 2016; Yao et al., 2008). Each time domain cross-correlation function is obtained by cross-correlating two vertical-component noise data with a sampling rate of 5 Hz. Preceding the cross-correlation, traditional signal processing such as removal of trend, mean, and instrument response (Bensen et al., 2007) are applied to the raw

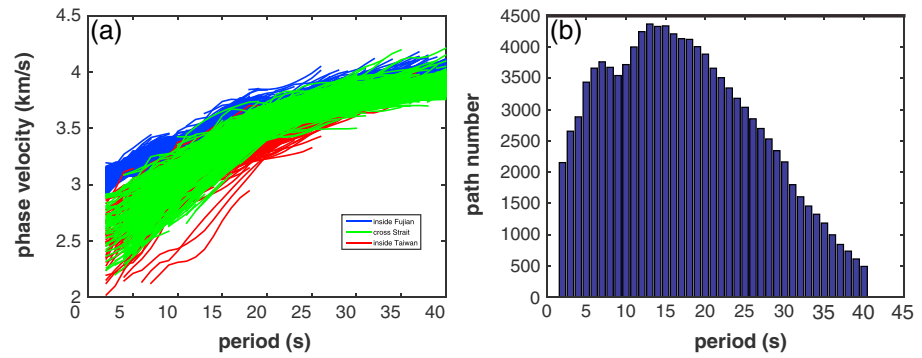


Figure 2. (a) Rayleigh wave phase velocity dispersion curves for different regions. Blue lines denote dispersion data in the Fujian area; green, data crossing the strait; and red, data in Taiwan. (b) Number of phase velocity measurements at different periods.

data. Spectral whitening is then performed for each 2-hr-long segment waveform. Then, we take the multiple period band running-absolute-mean normalization to suppress the influence of predominant periods of noise and earthquake sources. The broadband normalized waveform can be written as

$$\widehat{S} = \sum_j S_j(T_j, T_{j+1}) / A(S_j(T_j, T_{j+1})), \quad (1)$$

where $S_j(T_j, T_{j+1})$ is the bandpass-filtered waveform in the j th period band $[T_j, T_{j+1}]$, and A denotes the running-mean-absolute amplitude of the waveform S_j using a window length of $2T_{j+1}$. Daily cross-correlation functions are then stacked for each station pair. With 2-years' stacking, surface-wave signals from ambient noise cross-correlation appear very stable with high signal-to-noise ratios.

An image transformation method (Yao et al., 2006, 2011) is used to extract the fundamental mode Rayleigh wave group and phase velocity dispersion curves in the period range of 2 to 40 s. In consideration of the far-field assumption of surface wave propagation (Yao et al., 2006, 2011), we require that the interstation distance should be at least 2 times larger than the wavelength at each period. Dispersion data with large deviations or irregular shapes are removed. We take cluster analysis of the dispersion curves to eliminate those dispersion data that have similar paths but quite different measurements with respect to their mean (see supporting information and Figure S1). Finally, we obtain more than 4,000 dispersion curves. The number of measurements decreases rapidly for periods greater than 25 s (Figure 2b).

Dispersion data across different regions differ greatly, especially at short periods (Figure 2a). Due to the water and sedimentary layers, measurements with periods less than 10 s across the strait are lower than those in the Fujian area. Moreover, we observe anomalously low phase velocities at short periods in Taiwan, which may imply low shear-wave velocity in the upper crust, in particular, the southwestern part of Taiwan. The 2π ambiguity problem and the low-velocity structure make it difficult to identify the correct very short period phase-velocity branches for some paths.

2.2. Methodology for Direct Surface-Wave Tomography

We adopt the direct surface-wave tomography method (Fang et al., 2015; C. Li et al., 2016), in which an intermediate step of inversion for phase or group velocity maps is not required, to invert all period-dependent surface-wave traveltimes data for 3-D variations in subsurface shear-wave velocity structures. To calculate Rayleigh wave traveltimes at a certain period, a 2-D fast marching method (Rawlinson & Sambridge, 2004) is used without the assumption of great-circle path propagation using the corresponding phase velocity map predicted from a 3-D velocity model. Following Fang et al. (2015), the frequency-dependent surface wave traveltime $t(\omega)$ can be written as

$$t_i(\omega) = \sum_{p=1}^P S_p^{(i)}(\omega) \Delta l_i = \sum_{p=1}^P \sum_{k=1}^K v_{pk}^{(i)} \widehat{S}_k(\omega) \Delta l_i = \sum_{k=1}^K v_{ik} \widehat{S}_k(\omega), \quad (2)$$

where $S_p^{(i)}(\omega)$ represents the slowness for a segment p along path i in lengths of Δl_i . If we discretize a 2-D slowness model in the whole study region, the slowness can be expressed in terms of a bilinear interpolation of all

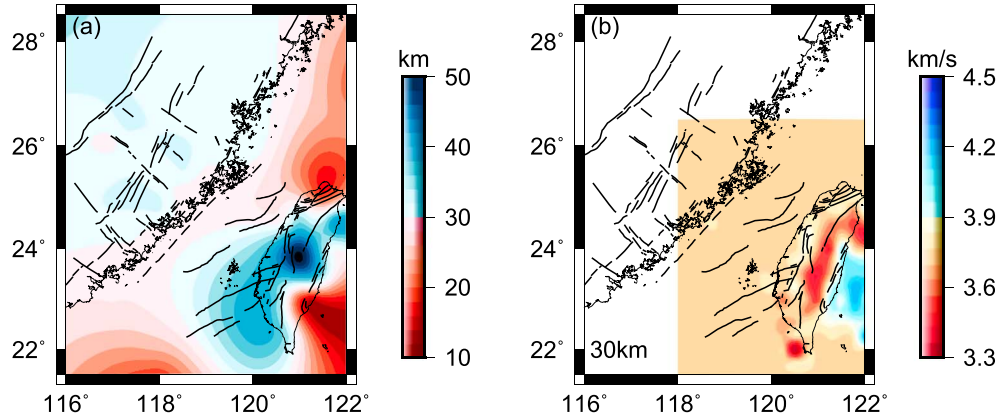


Figure 3. Initial model settings for the inversion. (a) Moho depth of the study region from He et al. (2014). (b) Tomography result of V_s at 30-km depth from Kuo-Chen, Wu, Jenkins, et al. (2012). We take the Moho depth information for the NW part of the initial model and Kuo-Chen's model for the Taiwan part.

the slownesses $\widehat{S}_k(\omega)$ ($k = 1, 2, \dots, K$) at the predefined regular grids, where k denotes the index of the regular grid point of the model, K is the total number of points, and $v_{pk}^{(i)}$ represents the interpolation coefficients along a given path i . Furthermore, we can combine $\sum_{p=1}^P v_{pk}^{(i)} \Delta l_i$ into v_{ik} , which has been associated with the i th traveltimes data.

An optimal model can be obtained by minimizing the differences between the observed traveltimes $t_i^{\text{obs}}(\omega)$ and predicted traveltimes $t_i^{\text{pred}}(\omega)$ calculated from the reference model for all frequencies ω , that is,

$$\delta t_i(\omega) = t_i^{\text{obs}}(\omega) - t_i^{\text{pred}}(\omega) = \sum_{k=1}^K v_{ik} \delta \widehat{S}_k(\omega) \approx - \sum_{k=1}^K v_{ik} \frac{\delta C_k(\omega)}{C_k^2(\omega)}. \quad (3)$$

We can update the predicted traveltimes when a new model is obtained in the iterative inversion. C_k is either the phase or group velocity, and δC_k is its perturbation of the k th grid point. Since the phase or group velocity is sensitive to compressional wave velocity α , shear wave velocity β , and density ρ , the perturbation of C_k can be expressed by an integral of partial derivatives of the three parameters:

$$\delta C_k(\omega) = \int \left[\frac{\partial C_k(\omega)}{\partial \alpha_k(z)} \Big|_{\theta_k} \delta \alpha_k(z) + \frac{\partial C_k(\omega)}{\partial \beta_k(z)} \Big|_{\theta_k} \delta \beta_k(z) + \frac{\partial C_k(\omega)}{\partial \rho_k(z)} \Big|_{\theta_k} \delta \rho_k(z) \right] dz, \quad (4)$$

where θ_k denotes the 1-D layered reference model. We can use a simple difference method to calculate the sensitivities of phase or group velocity to each parameter at a given depth grid point (Fang et al., 2015). Considering that surface wave dispersion is mostly sensitive to shear-wave velocity, we relate compressional wave velocity and density to shear-wave velocity using the empirical relationships given by Brocher (2005). Thus, equation (3) can be transformed to

$$\delta t_i(\omega) = \sum_{k=1}^K \left(-\frac{v_{ik}}{C_k^2} \right) \sum_{j=1}^J \left[R'_\alpha(z_j) \frac{\partial C_k}{\partial \alpha_k(z_j)} + R'_\rho(z_j) \frac{\partial C_k}{\partial \rho_k(z_j)} + \frac{\partial C_k}{\partial \beta_k(z_j)} \right] \Big|_{\theta_k} \delta \beta_k(z_j) = \sum_{l=1}^M G_{il} m_l, \quad (5)$$

where R'_α and R'_ρ are the scaling factors relating the perturbation of compressional wave speed and density, respectively, to the perturbation of shear-wave velocity (see Fang et al., 2015, in detail), J is number of grid nodes in the depth direction, and $M = KJ$, which is the total number of grid points of the 3-D model. Accordingly, we can solve the classical inversion function $\mathbf{d} = \mathbf{Gm}$ using LSQR (Paige & Saunders, 1982). The data sensitivity matrix G consisting of the three items can be calculated from the initial model, which is updated in the iteration. To stabilize the inversion, we add a spatial smoothing term with the first-order Tikhonov model regularization (Aster et al., 2013).

In this study, we mainly focus on the tectonics of the strait and Fujian. Since the data coverage in Taiwan is too sparse to reveal small-scale structures, we take the regional and high-resolution S wave velocity model in

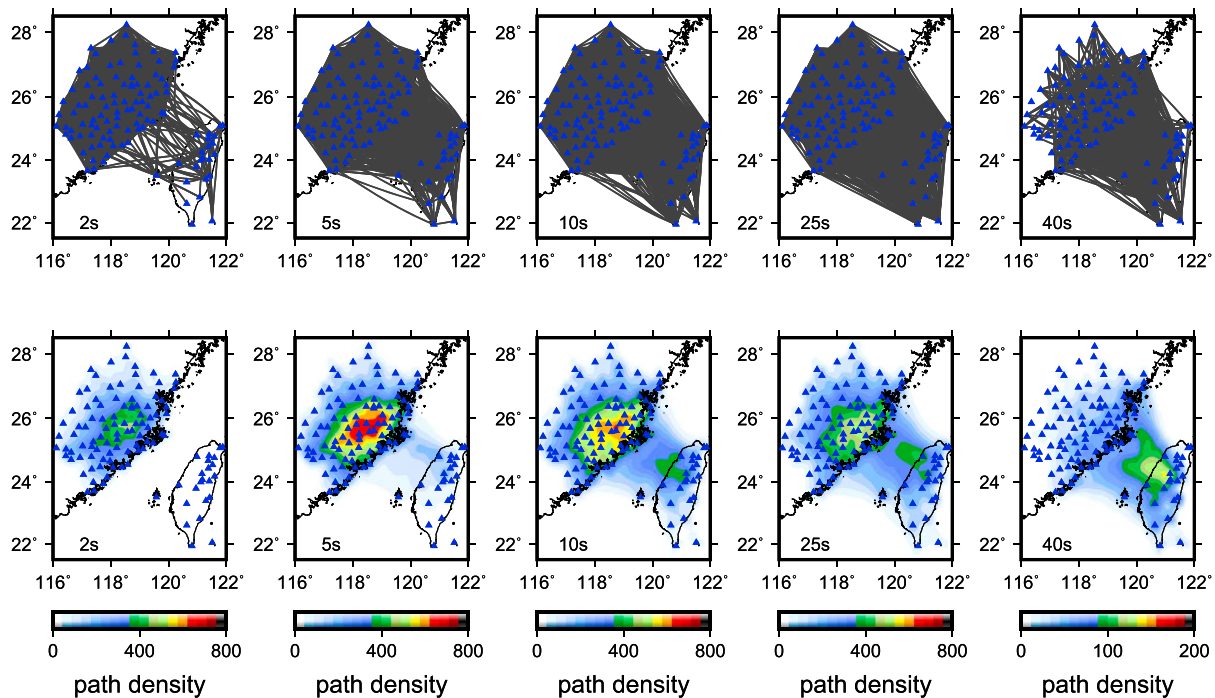


Figure 4. Ray path coverage (top) and density (bottom) for the final 3-D model at different periods. Blue triangles denote stations.

Taiwan from Kuo-Chen, Wu, Jenkins, et al. (2012) as part of our initial model (Figure 3b). As surface waves are not sensitive to interface geometry, we also add the information on the Moho depth from He et al. (2014) to the rest of our initial model (Figure 3a).

3. Path Coverage and Resolution Tests

The path coverage of phase velocity measurements (Figure 4) is quite good in a period range of 5–35 s across the whole region. In addition, the Fujian area presents good spatial coverage at short periods of 2–5 s. Bending ray paths are observed at short periods due to a strong velocity anomaly in the shallow crust (also see Figure S2).

To assess the spatial resolution and the robustness of the inversion results at different depths, we perform checkerboard tests using different anomaly sizes. Anomalies are superimposed on a reasonable 1-D model, and we choose a size of 0.75° by 0.75° to show the real model (Figure 5a). Recovered structures at different depths are shown in Figures 5b–5f, revealing that the lateral resolution in the Fujian area is approximately 60–80 km and in the strait and Taiwan, approximately 80–120 km. Slight smearing along the direction perpendicular to the strait still exists due to the distribution of many cross-strait ray paths. For the vertical resolution, the checkerboard pattern can be recovered well from the surface to at least the top of the upper mantle (Figure 6).

4. Results

We select the inverted shear-velocity images at depths of 10, 20, 30, and 40 km in the study region (Figure 7). Moreover, due to good path coverage in the Fujian area even at short periods, we also display shallow crustal structures at depths shallower than 10 km (Figure 8). The prior Moho depth imposed in our initial model could strongly influence the shear-wave velocity structure around the Moho depth if the initial Moho depth is very different from the true value, for example, in the Taiwan area (see the inversion results using the flat initial Moho in Figures S3 and S4). Since we do not have very good constraints on upper mantle structures due to the period range limit (2–40 s) of the used dispersion data, we mainly focus on crustal and uppermost mantle structures (to approximately 40-km depth) in the study region.

At depths shallower than 10 km (Figures 7a and 8a–8c), the Fujian area displays a high-velocity anomaly in the north and a low-velocity anomaly in the south, especially in the uppermost crust (Figure 8a). Basins

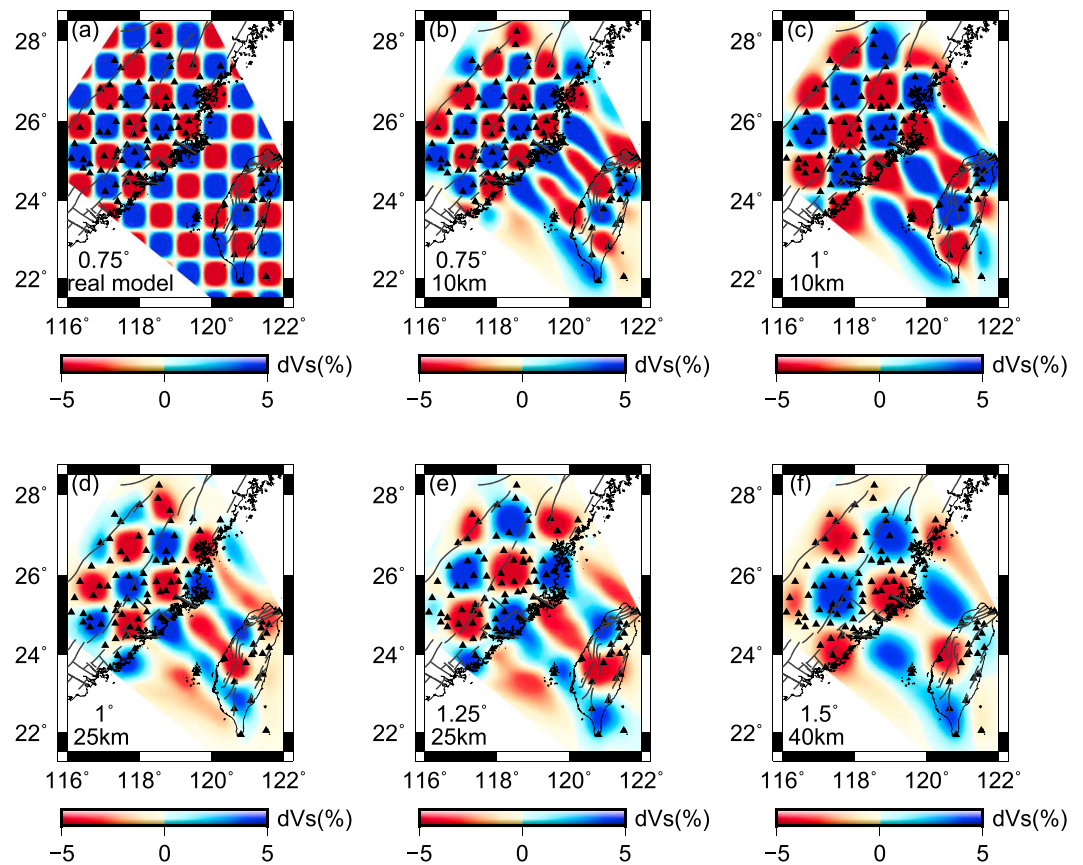


Figure 5. Horizontal slices of the checkerboard resolution tests. (a) Input real checkerboard model with the anomaly size (0.75°) as shown in the upper left. The maximum strength of the shear-wave velocity anomaly is $\pm 5\%$. (b–f) Model recovery of different anomaly sizes at different depths. Black triangles show the locations of stations.

around Fuzhou and Zhangzhou show low-velocity features (Figure 10c). To a 10-km depth, the high-velocity anomaly appears predominately along the coastline of Fujian corresponding to west of the FLF (Figures 7a and 8c). Shear-wave velocities are slower to the west of the ZH-DP suture zone than to the east and abruptly decrease across the FLF. To the east of the FLF, extensional basins in the strait display relatively slow velocity anomalies compared to the velocity around Penghu Island in the southern part of the strait (Figure 10c). The lowest shear-wave velocity features are confined to the southwestern part of Taiwan and TNB, whereas the Central Range in Taiwan exhibits a high-velocity anomaly (Figure 7a). Most earthquakes occur around the junction zones of differently oriented fault zones (inland) and the boundaries between the high-velocity and low-velocity regions (in the strait).

At 20-km depth (Figures 7b and 8d), the spatial pattern of the velocity anomaly is nearly opposite to the pattern at 10-km depth. An approximately N-S-trending high-velocity belt, starting from the region northeast of Pingtan Island, Nanjihtao Basin (NJB), to Penghu-Beigang Uplift (see Figure 1 for the locations), can be extended to a depth of 30 km. In addition, seismicity along the coastline of Fujian and along the FLF becomes intensive (Figure 8d). We also observe a low-velocity corridor along the ZH-DP suture zone (Figures 7b, 8d, and 10b), consistent with the body-wave tomographic result of Cai et al. (2015), but this slow anomaly as well as the seismicity disappears at greater depths (Figure 8e). At a depth of 40 km (Figure 8f), the central region of Fujian and extensional basins in the strait are dominated by high shear-wave velocities, indicative of the uppermost mantle structure.

5. Discussion

We observe strong lateral variations in the continental crustal region of Fujian and Taiwan Strait. The most significant features include the low-velocity zone in the middle crust beneath the ZH-DP suture zone and

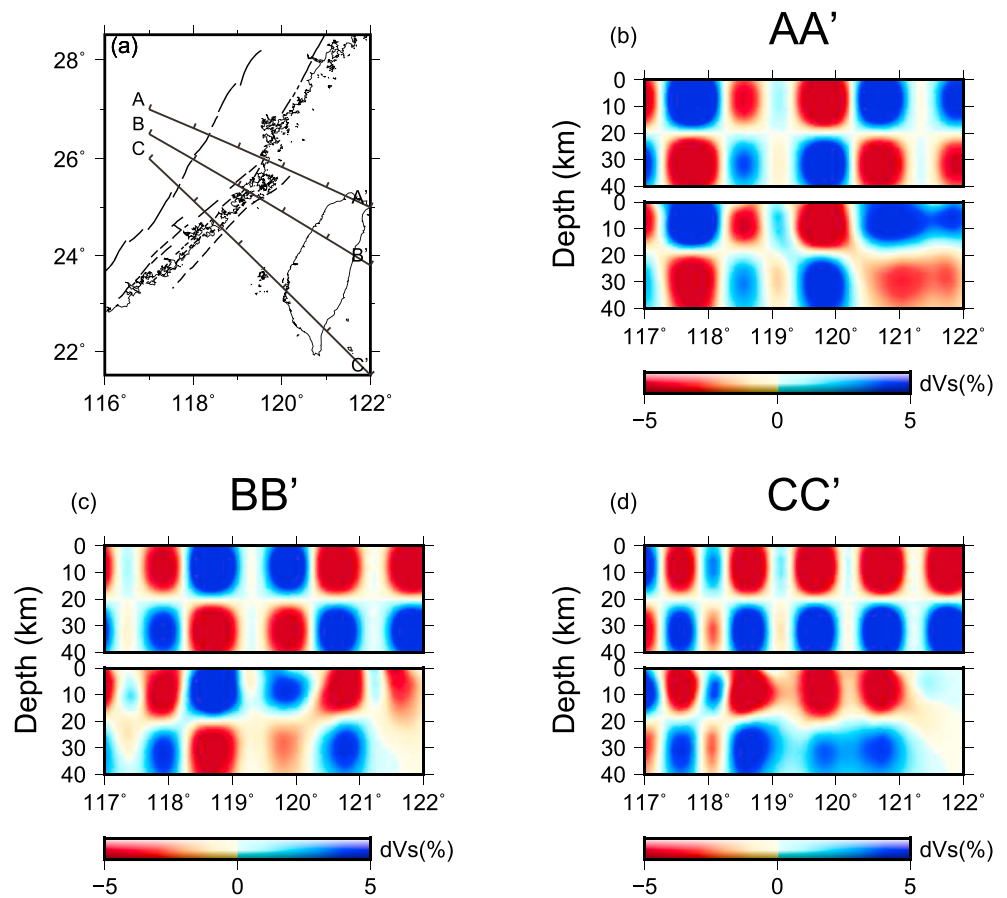


Figure 6. Vertical cross sections of the checkerboard tests. (a) Map with the location of three sections across the strait, which is also used in Figure 9. Simplified Zhenghe-Dapu, Changle-Zhaoan, and Fujian littoral fault are plotted. (b–d) Input real (top) and recovered (bottom) vertical cross sections along the three transects in (a). The size of each block anomaly is approximately 20 km in depth and 100 km in the horizontal direction. Note that the adjacent anomaly blocks do not have the same horizontal size due to the slanted lines in (a).

the high-velocity zones in the upper crust along the coast of Fujian as well as from the middle crust to the uppermost mantle in the strait (Figures 7 and 9). The general pattern of our tomographic results from ambient noise tomography is generally consistent with the previous results using different data sets and/or methods (Cai et al., 2015; Z. Huang et al., 2010; Kuo et al., 2015; H. W. Zheng et al., 2013), but our results can resolve more details, which is discussed later.

5.1. The Tectonic Implication of Structural Results in and Around Fujian

In the Fujian area, the high-velocity zone appears in the north, and the low-velocity zone dominates in the south at shallow depths (Figures 8a and 8b). Liang et al. (2012) thought this velocity contrast might coincide well with mountain ranges in the north and downfaulted basins in the south. However, this interpretation appears not very obvious from topography (see Figure 1b). More earthquakes and faults are concentrated in southern Fujian (Figures 1a, 8a, and 8b), which reflects more active and fragmented strata there, and in our view, this fragmentation is probably the main cause of the slower velocity structure in southern Fujian. The crustal structure at 10-km depth is characterized by several small blocks with different shear-wave velocities demarcated by the NW-SE- and NE-SW-trending faults of which the ZH-DP suture zone is the most significant (Figure 8). Separated by this ZH-DP suture zone, the eastern and western parts of the middle to lower crust have distinct velocity structures characterized by relatively low speed in the west and high speed in the east (Figures 8c and 8d). Previous *P* wave studies based on deep seismic sounding (Cai et al., 2015; Kuo et al., 2015; P. Li et al., 2015) also show similar features and indicate that the velocity contrast could be related to strata of different ages and the resulting variations in composition because of the different experiences of

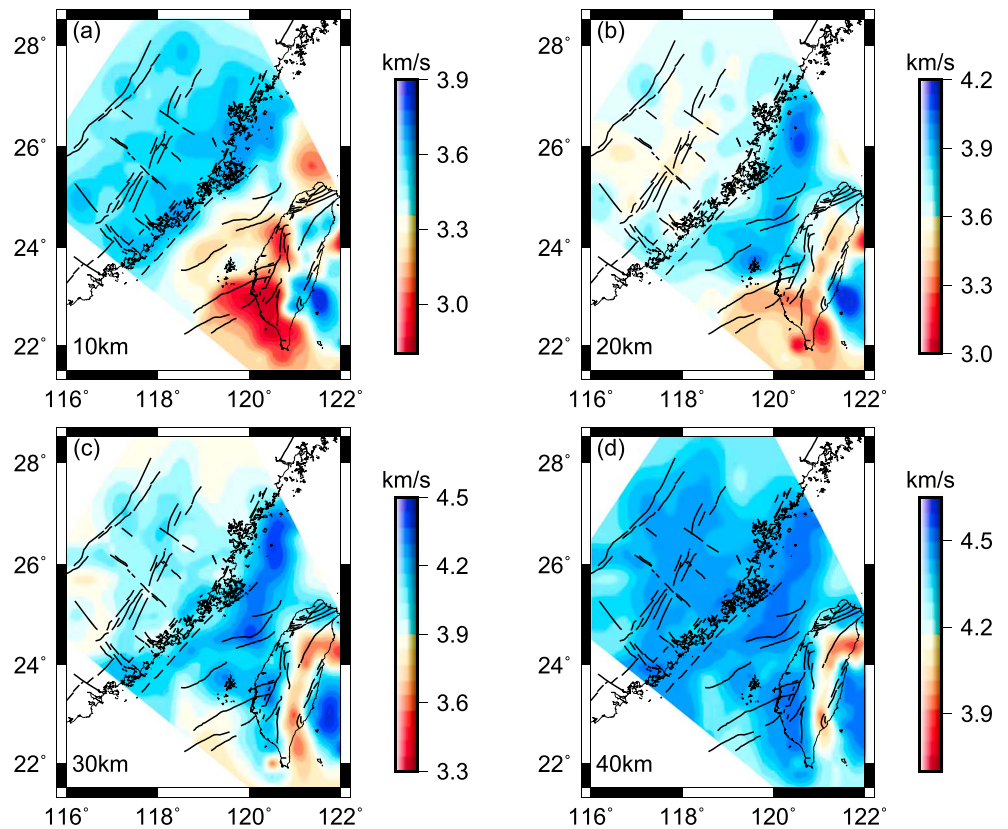


Figure 7. Map views of shear-wave velocity at four different depths: 10, 20, 30, and 40 km. The black lines denote the faults in the region. The dashed line denotes the Fujian littoral fault.

tectonic activity. The western Fujian area is part of the Southeast China Caledonian fold belt of the Cathaysia block (T. K. Huang, 1978) and has been deformed by three tectonic events, including the Caledonian (J. Chen & Jahn, 1998; S. Wang et al., 2017), Indosinian (Xu et al., 2007), and early Yanshanian movements (X. H. Li, 2000). The eastern Fujian area, in contrast, is recognized as a different tectonic unit in the Cathaysia block, namely, the Southeast Maritime Fold Belt (T. K. Huang, 1978), which was mainly influenced by the late Yanshanian movement (Zhou et al., 2006). The late Yanshanian magmatism due to the subduction and retreat of the paleo-Pacific plate (Z. X. Li & Li, 2007; Z. Li et al., 2014) overprinted on the Paleoproterozoic crustal basement (Xu et al., 2007) in eastern Fujian and produced widespread igneous rocks. The cooled igneous rocks, which contain more mafic materials compared to the felsic materials in the basement, may account for the high-velocity structures. The exceptions are the basins near Fuzhou and Zhangzhou that show lower velocity features at shallow depths (Figures 8a and 8b) that may due to the relatively thicker sediments and high heat flow (Hu et al., 2000; Y. Wang, 2001). However, Figure 10c shows that the low-velocity region may extend to the middle crust. The region around the Zhangzhou Basin has many faults and earthquakes (Figure 8), which probably lead to a fractured and thus slow upper-middle crust. There are many hot springs in the Fuzhou area; thus, the low-velocity anomaly beneath Fuzhou Basin is probably as the result of a high geothermal gradient. The seismicity is mainly located in southern and eastern Fujian and the strait (Figure 8), particularly at the junction of faults and in regions with remarkable velocity changes. This result implies that seismicity could depict the boundaries of geological structures with different rigidities.

In addition, we observe slow anomalies beneath the ZH-DP suture zone that extend to the lower crust and thus infer that this suture zone is deeply rooted in the crust (Kuo et al., 2015). X. Li (2013) proposed a conjunctive zone in central Fujian, which resulted from the closing of a paleo-ocean in central Fujian. Moreover, the appearance of ophiolite mélangé, pelagic sedimentary rocks, and basaltic debris at the surface around the ZH-DP suture zone indicates that the low velocity in the middle crust of this region may be linked to the remnants of an ancient oceanic basin (Kuo et al., 2015; X. Li, 2013). Although the whole Southeast China Block was

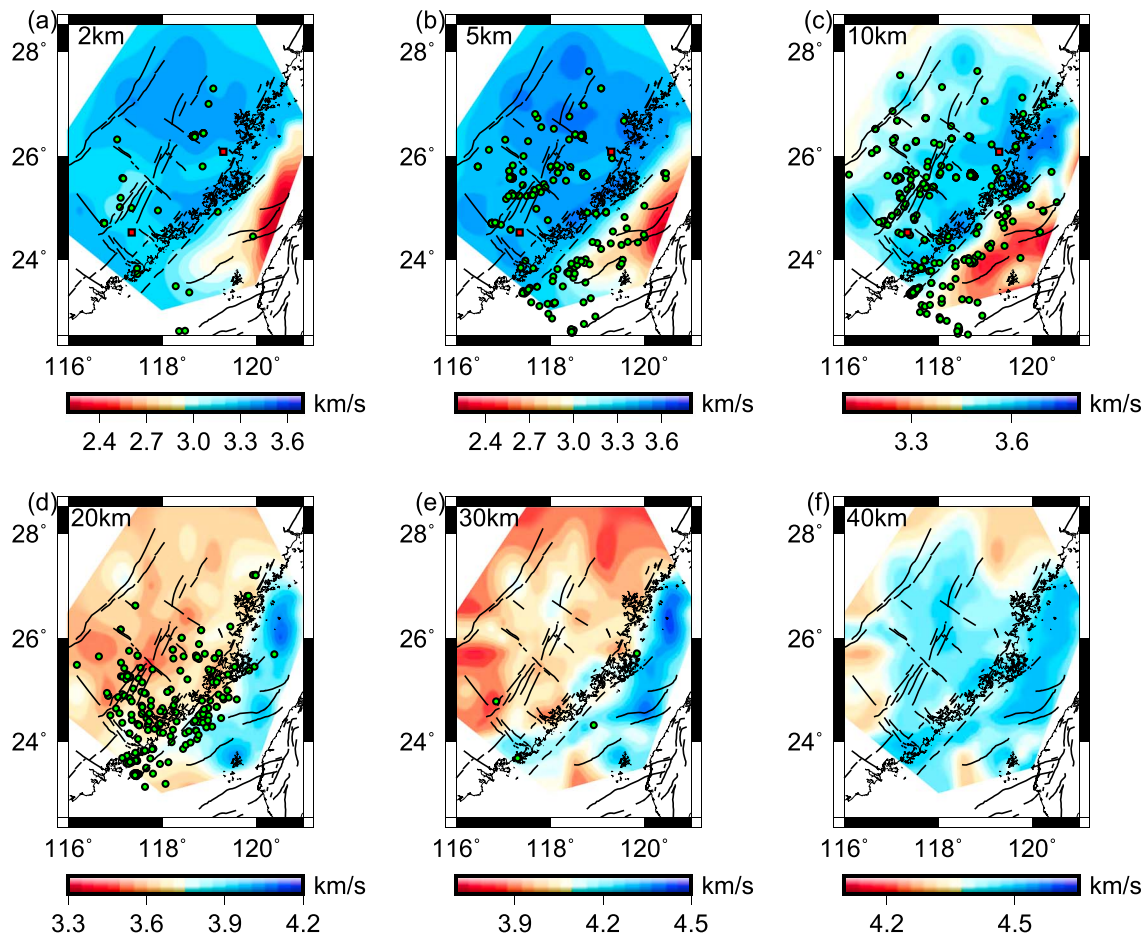


Figure 8. Map views of shear-wave velocity in Fujian and Taiwan Strait with regional seismicity (green circles) at six different depths: 2, 5, 10, 20, 30, and 40 km. The time range of the seismicity is 2008–2016 with magnitudes $M_s > 1$. For the velocity map at each depth, only earthquakes having focal depths within ± 1 km of that depth are plotted. The black lines denote faults in the region. The dashed line in the Taiwan Strait indicates the Fujian littoral fault. The two red squares denote the two cities: Fuzhou (north) and Zhangzhou (south).

preliminarily united at the later stage of the Early Paleozoic (J. Chen & Jahn, 1998; Shu et al., 2015), Xu et al. (2007) suggested that east and west Cathaysia, bounded by ZH-DP suture zone, were separated before the Indosinian event as evidenced by the lack of Caledonian and Indosinian magmatic suites in eastern Cathaysia.

The high-velocity zone in the upper crust along the coast of Fujian, which is conspicuously distributed between the CL-ZA fault zone and FLF (Figures 7 and 8), is also found in the results of Cai et al. (2015) and K. X. Chen et al. (2016). The anomalously high velocity in the upper crust coincides well with the PDMB, which predominately consists of granites and amphibolite-facies metamorphic rocks (W. S. Chen et al., 2002; Liu et al., 2012). Most of the Yanshanian granites in the PDMB exhibit arc-related affinities in trace element and isotope compositions (Liu et al., 2012). Based on the structural analysis, the PDMB and its surrounding region experienced strong shearing in the Early Cretaceous, and coeval NW-directed thrusts were developed (Wei et al., 2015); that is, the CL-ZA fault served as a ductile backthrust. Both the formation and deformation of the PDMB could have occurred in response to the northwestward to northward subduction of the paleo-Pacific plate (W. S. Chen et al., 2002; Liu et al., 2012; Y. T. Yang, 2013), which produced a high-pressure metamorphic environment and was presumably followed by collision with a microcontinent (Wei et al., 2015) or the Philippine plate (Jahn et al., 1990).

The compressional tectonics corresponding to the collision then changed to an extensional environment in the late Mesozoic as revealed by the appearance of bimodal volcanic rocks (Z. Li et al., 2014; Zhou et al., 2006), A-type granites (X. H. Li, 2000; Qiu et al., 2004; Zhao et al., 2015), mafic dike swarms (S. Wang et al., 2017), and extensional or rift basins (Shu et al., 2004; D. Wang & Shu, 2012). Cenozoic extension due to the opening and

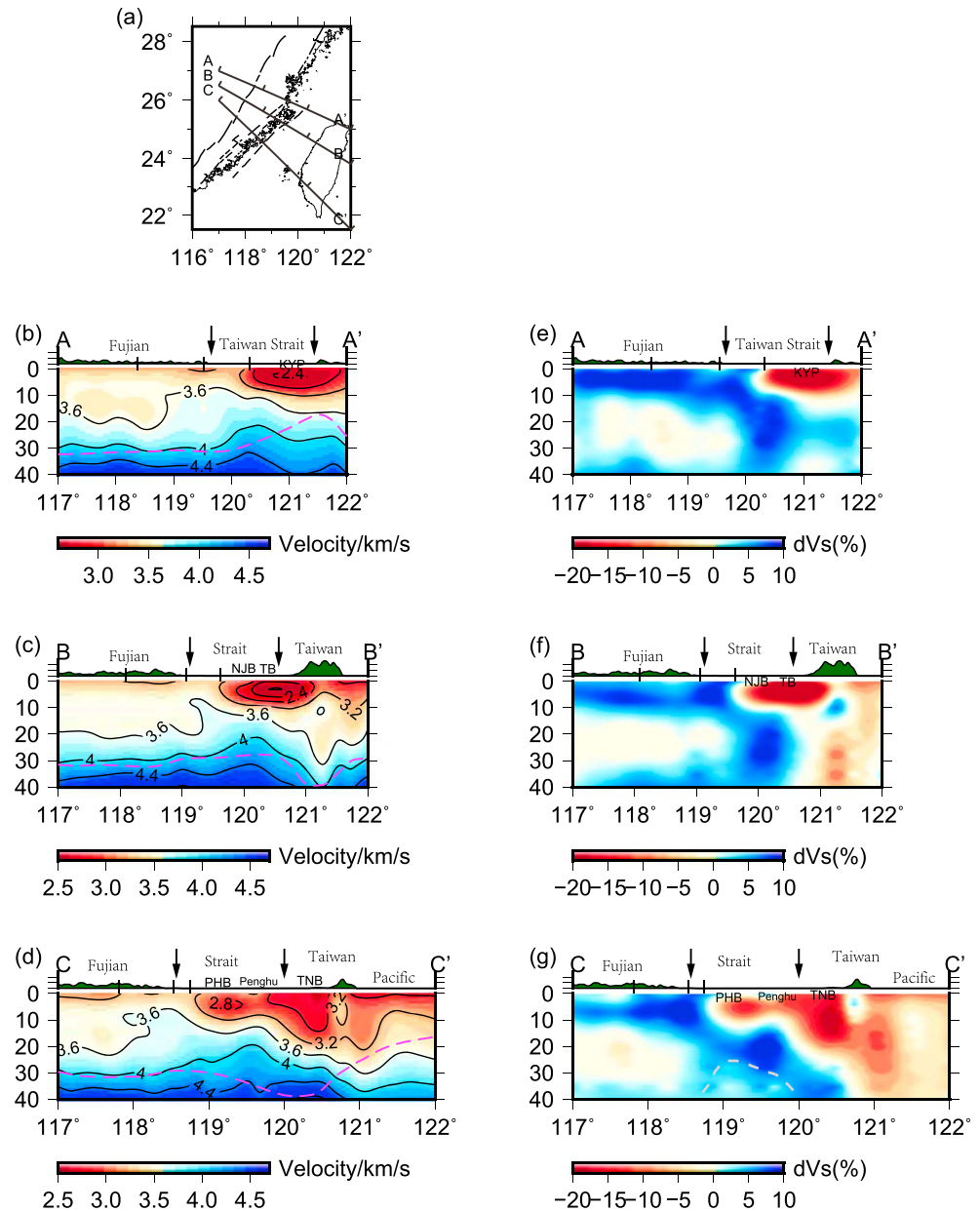


Figure 9. Cross sections of shear-wave velocity along three different profiles at the locations shown in (a). (b–d) Absolute values of shear-wave velocity. The seismic Moho is approximately delineated by the 4-km/s contour of shear-wave velocity. Gray-dashed lines indicate the Moho interface from He et al. (2014). (e–g) Perturbations of shear-wave velocity (in percent) relative to the average 1-D model in the study area. Black arrows denote the coastlines, and the black bars from left to right indicate the locations of the Zhenghe-Dapu suture, Changle-Zhaoan fault, and Fujian littoral fault. KYP = Kuanyin platform; NJJB = Nanjihtao Basin; TB = Taihsi Basin; PHB = Penghu Basin; TNB = Tainan Basin.

migration of the South China Sea also resulted in sporadic magmatism around the southern CL-ZA fault (Ho et al., 2003; X. Li, 2013). Despite the fact that the Late Cretaceous and Cenozoic magmatism could have modified subsurface structures, the geometry of the high-velocity zone along the coast highly correlates with the PDMB, indicating that the seismic anomaly is dominated by the late Yanshanian magmatic rocks that formed in a compressional environment and were coeval with uplifted metamorphic rocks.

5.2. Geological Interpretations of the Tomographic Results in and Around the Strait

The Taiwan Strait is filled with Cenozoic sediments showing low-velocity anomalies and extending to approximately 10-km depth except for Penghu Island (Figures 7a and 9). The crustal thickness of the strait

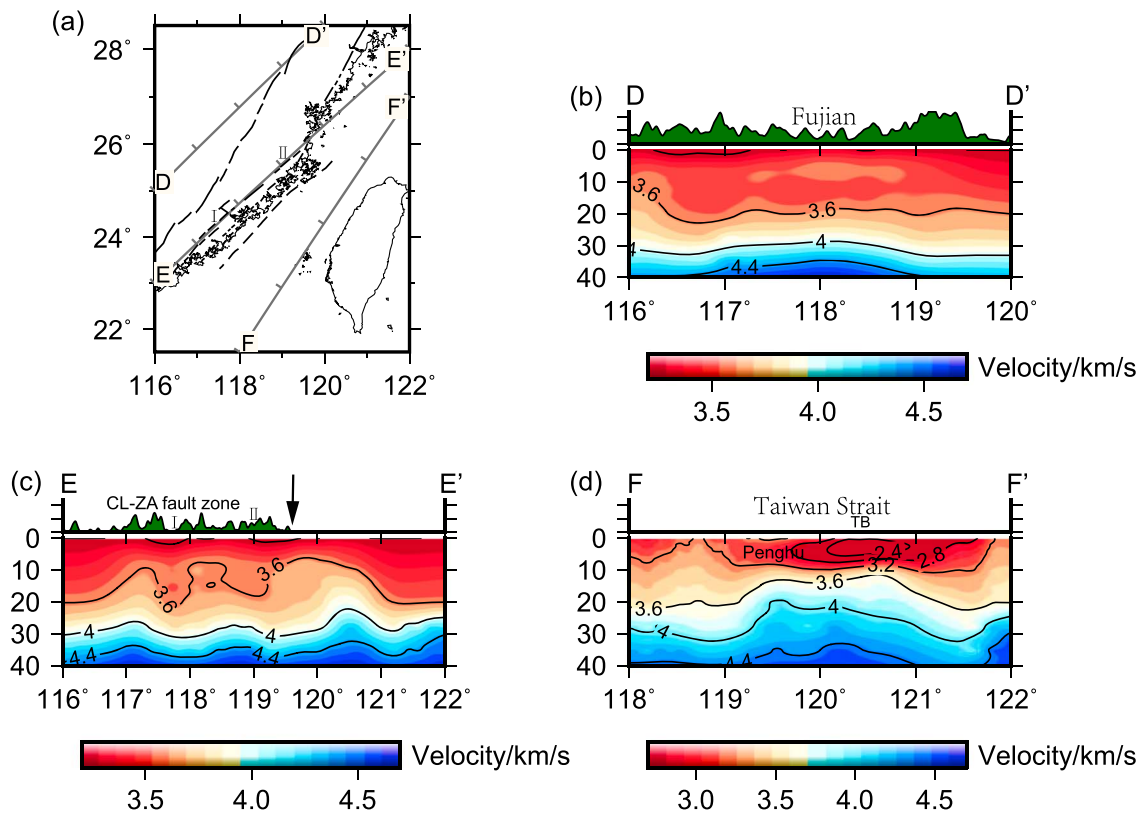


Figure 10. Cross sections of shear-wave velocity subparallel to the continental margin. (a) Map with the locations of the three sections. (b–d) Shear-wave velocities along the three different profiles in (a). I = Zhangzhou Basin; II = Fuzhou Basin; TB = Taihsi Basin. Black arrow denotes the coastline. Note that the color scale for profile FF' is different from the scales in (b) and (c). CL-ZA = Changle-Zhaoan.

is less than 30 km (Figure 9), similar to that of global extended continental crust (Christensen & Mooney, 1995). Both features can be explained by extension in the Cenozoic, which also resulted in high-velocity anomalies from the middle crust to uppermost mantle (Figures 7, 9, and 10). The extension along with the rifting tectonism led to the evolution of fault-bounded basins such as the NJB, Penghu Basin (PHB), and TNB. Igneous rocks are generated by decompression melting of hot mantle material as it rises passively beneath the extended and thinned lithosphere (White & McKenzie, 1989). Crustal uplift and vigorous mantle-derived magmatism, which resulted in extrusive igneous bodies and underplated igneous rocks, occurred during the extension along with the induced sedimentary basins (Chung et al., 1994).

The NE-SW-oriented high-velocity zone in the mid-crust to upper mantle of the strait coincides well with the architecture of the ES margin, which has been influenced by the opening of the South China Sea (A. T. Lin et al., 2003). Rifting during the Paleogene accompanied by widespread intrusion of igneous rocks was mainly concentrated around the central and northern part of the strait such as the PHB, NJB, and Taihsi Basin. The igneous rocks have been overlain by several kilometers of sediments in the Cenozoic (A. T. Lin et al., 2003). Considering that the location and depth range of low-velocity anomalies in the strait approximately matches the Cenozoic sediment isopachs, we can deduce that the geological framework of this region was mainly influenced by Paleogene tectonics. Figures 9b–9d shows that all the high-velocity anomalies at depths of 10–35 km are distributed beneath the western low-velocity anomalies, which may imply that the middle to lower crust experienced magmatism or metamorphism during or after the extensional event.

In the southern part of the strait, a relatively high-velocity zone from the near surface to 40-km depth beneath Penghu Island extends eastward to the Peikang High (Figure 7), north of the TNB. This distinctive feature shows significant contrast with the widespread low-velocity anomalies in the southwest (Figures 7a and 7b) and central (Figures 7c and 7d) parts of Taiwan, which are accounted for by the sedimentary basin and thickening of the crust, respectively (H. H. Huang, Wu, Song, Chang, Lee, et al., 2014; T. Y. Huang et al., 2015; Kuo-Chen, Wu, & Roecker, 2012). The extension in the late Cenozoic produced strong intraplate

basaltic magmatism on the Penghu Islands, and the volcanism ceased at ~8 Ma because of compression due to the arc-continent collision in Taiwan (Chung et al., 1994). K. X. Chen et al. (2016) interpreted the velocity high as a basaltic edifice built during the lava extrusion. Beneath the high-velocity layer, they also observed a low-velocity zone in the depth range of the lower crust to upper mantle, indicating a cooling melt reservoir and magma feeder system. In our study, aside from the triangular-shaped, relatively slow anomaly in the deeper crust (depicted by the white line in Figure 9g) as revealed by K. X. Chen et al. (2016), a pronounced high-velocity anomaly just above the relatively slow one is also observed. Comparing the shapes of the high-velocity anomalies beneath basins in the northern strait (Figures 9e and 9f), we speculate the high-velocity anomaly in the south could have originated from the same Paleogene tectonic event as that in the north, which could be supported by the fact that the PHB is also a Paleogene syn-rift basin (A. T. Lin et al., 2003). In contrast with the northern strait, the PHB may have experienced Miocene magmatism that further modified the deeper crustal structure beneath. Thus, we conclude that the relatively slow anomaly may be attributed to the younger magmatism (Miocene), the temperature anomaly of which still remains, whereas the strong high-velocity anomaly is associated with the older magmatism (Paleogene).

In conclusion, two-stage extension with different centers in the early and late Cenozoic (A. T. Lin et al., 2003) and deposition could account for the main structural pattern. The first phase of lithospheric extension with discrete rifting occurred simultaneously centered mainly around the central and northern part of the strait, including the NJB, PHB, and Taihsi Basins, in the late Paleocene to Eocene. There may also have been slight magmatic activity along the coastline of Fujian, which resulted in the abundant geothermal resources in the eastern Fujian area (Figure 1a). In the Miocene, renewed extension moved southward to the northern depression of the TNB and induced basaltic volcanism beneath the Penghu Islands. Before extension was terminated by the compressional regime caused by the arc-continental collision, Penghu Island was formed by the upwelling of basaltic magma. The newly formed volcanic edifice beneath the older igneous rock formed in the Miocene appears as a relatively low-velocity anomaly.

To the southeast of the PHB, slow anomalies beneath TNB (or part of the coastal plain; Figures 9d and 9g) exhibit geometric patterns distinct from those beneath basins such as the PHB and Kuanyin platform in the strait. This contrast indicates that this region was dominated by other tectonic events than the Paleogene rift. Neogene rifting (postrift) and subsequent foreland depression due to the subduction-collision in Taiwan both yielded >10-km subsidence with the maximum depression taking place in the southeast (A. T. Lin et al., 2003), approximately consistent with our observation. Local body-wave tomography in Taiwan also reveals similar features in Pingtung Plain (e.g., H. H. Huang, Wu, Song, Chang, Lee, et al., 2014; Kuo-Chen, Wu, & Roecker, 2012). From south to north, the east terminations of the high-velocity anomalies beneath western Taiwan become steeper (Figures 9e–9g), which is consistent with the geometric variation in the subducted ES plate presented in H. H. Huang, Wu, Song, Chang, Kuo-Chen, et al. (2014). The authors interpreted the steep and complicated change as due to the involvement of the PHS slab in the northern part and its subduction beneath the ES plate.

We summarize our findings in these three NE-SW-trending transects (Figure 10), approximately parallel to the tectonic settings developed since the late Mesozoic. The geological units near the surface are younger toward the east; thus, structures beneath the profiles could be representative of the tectonic evolution in the study region. To the west of the ZH-DP suture, profile DD' located in the western Cathaysia block shows laterally similar structures in seismic images. In contrast, subsurface structures beneath the farther east profile EE' along the coastline of Fujian fluctuate and represent fast upper and middle crust (except beneath the two basins). The spatial seismic discrepancy can be attributed to different tectonic processes in different eras. The west profile (DD') was dominated by events from Paleozoic to Jurassic, whereas the east (EE') mainly experienced Cretaceous magmatism and strong compressional deformation, particularly along the coast (W. S. Chen et al., 2002; Wei et al., 2015). The time-spatial correlation suggests that thermal and petrologic anomalies imprinted in the crust caused by older tectonic events may have been dissipated and transported away so that no distinct seismic anomaly remains laterally and vertically. Profile FF' transects structures that mainly developed in the Cenozoic. Thick Paleogene syn-rift sedimentary sequences in rift basins such as Taihsi Basin (A. T. Lin et al., 2003) are characterized by low shear-wave velocities (<3 km/s). Moreover, the Moho depth underneath the basins is shallower than it is under the other inland profiles by approximately 10 km. Our observations provide seismic evidence that the Cenozoic extensional activity predominately took place in

the continental margin, especially in the strait and that extension of the upper crust was accompanied by (lower) crustal thinning.

6. Conclusion

In this study, we use more than 100 stations and the direct surface-wave tomography method to obtain a 3-D crustal shear-wave velocity model in the Taiwan Strait and Fujian, southeast China. Our results reveal a high-velocity northern part and low-velocity southern part of Fujian in the upper crust, which are interpreted as influenced by the tectonic stability of different parts of Fujian in terms of the distribution of active faults and seismicity. A low-velocity corridor appears in the middle crust beneath the ZH-DP suture zone, which might be linked to the remnants of an ancient oceanic basin. This suture zone also separates the Wuyi-Yunkai orogenic belt (created in the Paleozoic) to the west and the Mesozoic downfaulted zone to the east. The velocity decreases abruptly from the Fujian area to Taiwan Strait at shallow depths across the FLF because of the sediments in the strait and the high-velocity PDMB along the coast of Fujian. The seismicity of Fujian and the strait is mainly concentrated on the boundary belts of variously oriented faults and regions, with remarkable velocity changes in the upper and middle crust of the southeastern part.

The extensional basins in the strait bounded by many normal faults present relatively high-velocity anomalies in the middle to lower crust because of the thinning of the crust in the Cenozoic and the widespread intrusion of igneous rock. The Penghu Islands might have additionally undergone intraplate volcanism in the late Cenozoic, resulting in relatively high-velocity upper-middle crust compared to the low-velocity sedimentary structures in other parts of the strait and relatively low-velocity lower crust to upper mantle compared to other regions at the same depth in the strait, which have experienced extension in the early Cenozoic.

Acknowledgments

Waveform data in Fujian used in this study are available through the Data Centre of Fujian Earthquake Administration and Data Management Centre of China National Seismic Network at Institute of Geophysics, China Earthquake Administration (doi: 10.11998/SeisDmc/SN, <http://www.seisdmc.ac.cn>). Waveform data in Taiwan are provided by BATS (Broadband Array in Taiwan for Seismology, <http://bats.earth.sinica.edu.tw>, doi: 10.7914/SN/TW). Cross-functions and shear-wave velocity model can be found in <https://github.com/zhangyayun021/Fujian-Taiwan-Data>. Some inter-station phase-velocity dispersion curves among 23 BATS stations, 6 EAFP stations, and 16 SinoProbe stations are provided by K. X. Chen et al. (2016). This research is funded by the National Natural Science Foundation of China (41790464, 41474071, and 51678539). Hsin-Ying Yang is supported by the Strategic Priority Research Program of the Chinese Academy of Sciences under grant XDB18010304. Most figures were plotted using the GMT (the Generic Mapping Tools [<http://gmt.soest.hawaii.edu>]).

References

- Ai, Y., Chen, Q. F., Zeng, F., Hong, X., & Ye, W. (2007). The crust and upper mantle structure beneath southeastern China. *Earth and Planetary Science Letters*, 260(3–4), 549–563. <https://doi.org/10.1016/j.epsl.2007.06.009>
- Aster, R. C., Borchers, B., & Thurber, C. H. (2013). *Parameter estimation and inverse problems*. Waltham, MA: Academic Press.
- Bensen, G. D., Ritzwoller, M. H., Barmin, M. P., Levshin, A. L., Lin, F., Moschetti, M. P., et al. (2007). Processing seismic ambient noise data to obtain reliable broad-band surface wave dispersion measurements. *Geophysical Journal International*, 169(3), 1239–1260. <https://doi.org/10.1111/j.1365-246X.2007.03374.x>
- Bird, P. (2003). An updated digital model of plate boundaries. *Geochemistry, Geophysics, Geosystems*, 4(3), 1027. <https://doi.org/10.1029/2001GC000252>
- Brocher, T. M. (2005). Empirical relations between elastic wavespeeds and density in the Earth's crust. *Bulletin of the Seismological Society of America*, 95(6), 2081–2092. <https://doi.org/10.1785/0120050077>
- Cai, H. T., Jin, X., Wang, S. X., Li, P., & Chen, W. (2016). The crust structure and velocity structure characteristics beneath Ninghua-Datian-Hui'an [in Chinese with English abstract]. *Chinese Journal of Geophysics*, 59(1), 157–168.
- Cai, H. T., Kuo-Chen, H., Jin, X., Wang, C. Y., Huang, B. S., & Yen, H. Y. (2015). A three-dimensional Vp, Vs, and Vp/Vs crustal structure in Fujian, Southeast China, from active-and passive-source experiments. *Journal of Asian Earth Sciences*, 111, 517–527. <https://doi.org/10.1016/j.jseaes.2015.06.014>
- Chen, J., & Jahn, B. M. (1998). Crustal evolution of southeastern China: Nd and Sr isotopic evidence. *Tectonophysics*, 284(1–2), 101–133. [https://doi.org/10.1016/S0040-1951\(97\)00186-8](https://doi.org/10.1016/S0040-1951(97)00186-8)
- Chen, K. X., Kuo-Chen, H., Brown, D., Li, Q., Ye, Z., Liang, W. T., et al. (2016). Three-dimensional ambient noise tomography across the Taiwan Strait: The structure of a magma-poor rifted margin. *Tectonics*, 35, 1782–1792. <https://doi.org/10.1002/2015TC004097>
- Chen, W. S., Yang, H. C., Wang, X., & Huang, H. (2002). Tectonic setting and exhumation history of the Pingtan–Dongshan Metamorphic Belt along the coastal area, Fujian Province, Southeast China. *Journal of Asian Earth Sciences*, 20(7), 829–840. [https://doi.org/10.1016/S1367-9120\(01\)00066-9](https://doi.org/10.1016/S1367-9120(01)00066-9)
- Christensen, N. I., & Mooney, W. D. (1995). Seismic velocity structure and composition of the continental crust: A global view. *Journal of Geophysical Research*, 100(B6), 9761–9788. <https://doi.org/10.1029/95JB00259>
- Chung, S. L., Sun, S. S., Tu, K., Chen, C. H., & Lee, C. Y. (1994). Late Cenozoic basaltic volcanism around the Taiwan Strait, SE China: Product of lithosphere-asthenosphere interaction during continental extension. *Chemical Geology*, 112(1–2), 1–20. [https://doi.org/10.1016/0009-2541\(94\)90101-5](https://doi.org/10.1016/0009-2541(94)90101-5)
- Data Management Centre of China National Seismic Network (2007). Waveform data of China National Seismic Network. Institute of Geophysics, China Earthquake Administration. <https://doi.org/10.11998/SeisDmc/SN>, <http://www.seisdmc.ac.cn>
- Fang, H., Yao, H., Zhang, H., Huang, Y. C., & van der Hilst, R. D. (2015). Direct inversion of surface wave dispersion for three-dimensional shallow crustal structure based on ray tracing: Methodology and application. *Geophysical Journal International*, 201(3), 1251–1263. <https://doi.org/10.1093/gji/ggv080>
- Gao, T. J., & Huang, H. (1995). Tectonic characteristics and evolution of the Taiwan Strait. *Acta Geologica Sinica*, 8(1), 1–13. <https://doi.org/10.1111/j.1755-6724.1995.mp8001001.x>
- He, R., Shang, X., Yu, C., Zhang, H., & van der Hilst, R. D. (2014). A unified map of Moho depth and Vp/Vs ratio of continental China by receiver function analysis. *Geophysical Journal International*, 199(3), 1910–1918. <https://doi.org/10.1093/gji/ggu365>
- Ho, K. S., Chen, J. C., Lo, C. H., & Zhao, H. L. (2003). ⁴⁰Ar–³⁹Ar dating and geochemical characteristics of late Cenozoic basaltic rocks from the Zhejiang–Fujian region, SE China: Eruption ages, magma evolution and petrogenesis. *Chemical Geology*, 197(1–4), 287–318. [https://doi.org/10.1016/S0009-2541\(02\)00399-6](https://doi.org/10.1016/S0009-2541(02)00399-6)

- Hsieh, H. H., Yen, H. Y., & Shih, M. H. (2010). Moho depth derived from gravity data in the Taiwan Strait area. *Terrestrial, Atmospheric and Oceanic Sciences*, 21(2), 235–241. [https://doi.org/10.3319/TAO.2009.03.05.01\(T\)](https://doi.org/10.3319/TAO.2009.03.05.01(T))
- Hu, S., He, L., & Wang, J. (2000). Heat flow in the continental area of China: A new data set. *Earth and Planetary Science Letters*, 179(2), 407–419. [https://doi.org/10.1016/S0012-821X\(00\)00126-6](https://doi.org/10.1016/S0012-821X(00)00126-6)
- Huang, H. H., Wu, Y. M., Song, X., Chang, C. H., Kuo-Chen, H., & Lee, S. J. (2014). Investigating the lithospheric velocity structures beneath the Taiwan region by nonlinear joint inversion of local and teleseismic P wave data: Slab continuity and deflection. *Geophysical Research Letters*, 41, 6350–6357. <https://doi.org/10.1002/2014GL061115>
- Huang, H. H., Wu, Y. M., Song, X., Chang, C. H., Lee, S. J., Chang, T. M., & Hsieh, H. H. (2014). Joint Vp and Vs tomography of Taiwan: Implications for subduction-collision orogeny. *Earth and Planetary Science Letters*, 392, 177–191. <https://doi.org/10.1016/j.epsl.2014.02.026>
- Huang, T. K. (1978). An outline of the tectonic characteristics of China. *Acta Geologica Sinica*, 71, 611–635.
- Huang, T. Y., Gung, Y., Kuo, B. Y., Chiao, L. Y., & Chen, Y. N. (2015). Layered deformation in the Taiwan orogen. *Science*, 349(6249), 720–723. <https://doi.org/10.1126/science.aab1879>
- Huang, Y. C., Yao, H., Wu, F. T., Liang, W. T., Huang, B. S., Lin, C. H., & Wen, K. L. (2014). Crustal and upper mantle S-wave velocity structures across the Taiwan Strait from ambient seismic noise and teleseismic Rayleigh wave analyses. *Journal of Asian Earth Sciences*, 81, 38–52. <https://doi.org/10.1016/j.jseaes.2013.11.023>
- Huang, Z., Wang, L., Zhao, D., Xu, M., Mi, N., Yu, D., et al. (2010). Upper mantle structure and dynamics beneath Southeast China. *Physics of the Earth and Planetary Interiors*, 182(3–4), 161–169. <https://doi.org/10.1016/j.pepi.2010.07.010>
- Institute of Earth Sciences, Academia Sinica, Taiwan (1996). *Broadband Array in Taiwan for Seismology*. Taiwan: Institute of Earth Sciences, Academia Sinica. Other/Seismic Network. doi:<https://doi.org/10.7914/SN/TW>
- Jahn, B. M., Zhou, X. H., & Li, J. L. (1990). Formation and tectonic evolution of southeastern China and Taiwan: Isotopic and geochemical constraints. *Tectonophysics*, 183(1–4), 145–160. [https://doi.org/10.1016/0040-1951\(90\)90413-3](https://doi.org/10.1016/0040-1951(90)90413-3)
- Kuo, Y. W., Wang, C. Y., Kuo-Chen, H., Jin, X., Cai, H. T., Lin, J. Y., et al. (2015). Crustal structures from the Wuyi-Yunkai orogen to the Taiwan orogen: The onshore-offshore wide-angle seismic experiments of the TAIGER and ATSEE projects. *Tectonophysics*, 692, 164–180. <https://doi.org/10.1016/j.tecto.2015.09.014>
- Kuo-Chen, H., Wu, F. T., Jenkins, D. M., Mechie, J., Roecker, S. W., Wang, C. Y., & Huang, B. S. (2012). Seismic evidence for the α - β quartz transition beneath Taiwan from Vp/Vs tomography. *Geophysical Research Letters*, 39, L22032. <https://doi.org/10.1029/2012GL053649>
- Kuo-Chen, H., Wu, F. T., & Roecker, S. W. (2012). Three-dimensional P velocity structures of the lithosphere beneath Taiwan from the analysis of TAIGER and related seismic data sets. *Journal of Geophysical Research*, 117, B06306. <https://doi.org/10.1029/2011JB009108>
- Li, C., Yao, H., Fang, H., Huang, X., Wan, K., Zhang, H., & Wang, K. (2016). 3D near-surface shear-wave velocity structure from ambient-noise tomography and borehole data in the Hefei Urban Area, China. *Seismological Research Letters*, 87(4), 882–892. <https://doi.org/10.1785/S1525-0273-2015-0257>
- Li, P., Jin, X., Wang, S., & Cai, H. (2015). Crustal velocity structure of the Shaowu-Nanping-Pingtan transect through Fujian from deep seismic sounding-tectonic implications. *Science China Earth Sciences*, 58(12), 2188–2199. <https://doi.org/10.1007/s11430-015-5191-6>
- Li, X. (2013). Subdivision and characteristic of tectonic units in Fujian Province [in Chinese with English abstract]. *Global Geology*, 32(3), 549–557.
- Li, X. H. (2000). Cretaceous magmatism and lithospheric extension in Southeast China. *Journal of Asian Earth Sciences*, 18(3), 293–305. [https://doi.org/10.1016/S1367-9120\(99\)00060-7](https://doi.org/10.1016/S1367-9120(99)00060-7)
- Li, Z., Qiu, J. S., & Yang, X. M. (2014). A review of the geochronology and geochemistry of Late Yanshanian (Cretaceous) plutons along the Fujian coastal area of southeastern China: Implications for magma evolution related to slab break-off and rollback in the Cretaceous. *Earth-Science Reviews*, 128, 232–248. <https://doi.org/10.1016/j.earscirev.2013.09.007>
- Li, Z. X., & Li, X. H. (2007). Formation of the 1300-km-wide intracontinental orogen and postorogenic magmatic province in Mesozoic South China: A flat-slab subduction model. *Geology*, 35(2), 179–182. <https://doi.org/10.1130/G23193A.1>
- Liang, F. H., Jin, X., Li, J., Wang, S. C., Chen, C. X., & Wang, Z. Y. (2012). Surface wave tomography of ambient seismic noise correlation in Fujian Province [in Chinese with English abstract]. *Earthquake Research in China*, 28(1), 22–32.
- Lin, A. T., Watts, A., & Hesselbo, S. P. (2003). Cenozoic stratigraphy and subsidence history of the South China Sea margin in the Taiwan region. *Basin Research*, 15(4), 453–478. <https://doi.org/10.1046/j.1365-2117.2003.00215.x>
- Lin, A. T., & Watts, A. B. (2002). Origin of the West Taiwan basin by orogenic loading and flexure of a rifted continental margin. *Journal of Geophysical Research*, 107(B9), 2185. <https://doi.org/10.1029/2001JB000669>
- Lin, F.-C., Moschetti, M. P., & Ritzwoller, M. H. (2008). Surface wave tomography of the western United States from ambient seismic noise: Rayleigh and Love wave phase velocity maps. *Geophysical Journal International*, 173(1), 281–298. <https://doi.org/10.1111/j.1365-246X.2008.03720.x>
- Liu, Q., Yu, J. H., Wang, Q., Su, B., Zhou, M. F., Xu, H., & Cui, X. (2012). Ages and geochemistry of granites in the Pingtan–Dongshan Metamorphic Belt, Coastal South China: New constraints on Late Mesozoic magmatic evolution. *Lithos*, 150, 268–286. <https://doi.org/10.1016/j.lithos.2012.06.031>
- Paige, C. C., & Saunders, M. A. (1982). LSQR: An algorithm for sparse linear equations and sparse least squares. *ACM Transactions on Mathematical Software*, 8(1), 43–71. <https://doi.org/10.1145/355984.355989>
- Qiu, J. S., Wang, D. Z., McInnes, B. I., Jiang, S. Y., Wang, R. C., & Kanisawa, S. (2004). Two subgroups of A-type granites in the coastal area of Zhejiang and Fujian Provinces, SE China: Age and geochemical constraints on their petrogenesis. *Earth and Environmental Science Transactions of the Royal Society of Edinburgh*, 95(1–2), 227–236. <https://doi.org/10.1017/S0263593300001036>
- Rawlinson, N., & Sambridge, M. (2004). Wave front evolution in strongly heterogeneous layered media using the fast marching method. *Geophysical Journal International*, 156(3), 631–647. <https://doi.org/10.1111/j.1365-246X.2004.02153.x>
- Seno, T., & Kawanishi, Y. (2009). Reappraisal of the arc-arc collision in Taiwan. *Terrestrial, Atmospheric and Oceanic Sciences*, 20(4), 573–585. [https://doi.org/10.3319/TAO.2008.07.11.02\(TT\)](https://doi.org/10.3319/TAO.2008.07.11.02(TT))
- Shapiro, N. M., & Campillo, M. (2004). Emergence of broadband Rayleigh waves from correlations of the ambient seismic noise. *Geophysical Research Letters*, 31, L07614. <https://doi.org/10.1029/2004GL019491>
- Shu, L., Faure, M., Yu, J. H., & Jahn, B. M. (2011). Geochronological and geochemical features of the Cathaysia block (South China): New evidence for the Neoproterozoic breakup of Rodinia. *Precambrian Research*, 187(3–4), 263–276. <https://doi.org/10.1016/j.precamres.2011.03.003>
- Shu, L., Wang, B., Cawood, P. A., Santosh, M., & Xu, Z. (2015). Early Paleozoic and early Mesozoic intraplate tectonic and magmatic events in the Cathaysia Block, South China. *Tectonics*, 34, 1600–1621. <https://doi.org/10.1002/2015TC003835>
- Shu, L., Zhou, X., Deng, P., Yu, X., Wang, B., & Zu, F. (2004). Geological features and tectonic evolution of Meso-Cenozoic basins in southeastern China [in Chinese with English abstract]. *Geological Bulletin of China*, 23, 9–10.

- Wang, D., & Shu, L. (2012). Late Mesozoic basin and range tectonics and related magmatism in Southeast China. *Geoscience Frontiers*, 3(2), 109–124. <https://doi.org/10.1016/j.gsf.2011.11.007>
- Wang, P. Z., Chen, Y. A., Cao, B. T., Pan, J. D., & Wang, C. Y. (1993). Crust–upper-mantle structure and deep structural setting of Fujian province [in Chinese with English abstract]. *Geology of Fujian*, 12(2), 79–158.
- Wang, S., Zhang, D., Wu, G., Vatuva, A., Di, Y., Yan, P., et al. (2017). Late Paleozoic to Mesozoic extension in southwestern Fujian Province, South China: Geochemical, geochronological and Hf isotopic constraints from basic-intermediate dykes. *Geoscience Frontiers*, 8(3), 529–540. <https://doi.org/10.1016/j.gsf.2016.05.005>
- Wang, Y. (2001). Heat flow pattern and lateral variations of lithosphere strength in China mainland: Constraints on active deformation. *Physics of the Earth and Planetary Interiors*, 126(3–4), 121–146. [https://doi.org/10.1016/S0031-9201\(01\)00251-5](https://doi.org/10.1016/S0031-9201(01)00251-5)
- Wei, W., Faure, M., Chen, Y., Ji, W., Lin, W., Wang, Q., et al. (2015). Back-thrusting response of continental collision: Early Cretaceous NW-directed thrusting in the Changle-Nan'ao belt (Southeast China). *Journal of Asian Earth Sciences*, 100, 98–114. <https://doi.org/10.1016/j.jseas.2015.01.005>
- White, R., & McKenzie, D. (1989). Magmatism at rift zones: The generation of volcanic continental margins and flood basalts. *Journal of Geophysical Research*, 94(B6), 7685–7729. <https://doi.org/10.1029/JB094iB06p07685>
- Xu, X., O'Reilly, S. Y., Griffin, W. L., Wang, X., Pearson, N. J., & He, Z. (2007). The crust of Cathaysia: Age, assembly and reworking of two terranes. *Precambrian Research*, 158(1–2), 51–78. <https://doi.org/10.1016/j.precamres.2007.04.010>
- Yang, Y., Ritzwoller, M. H., Levshin, A. L., & Shapiro, N. M. (2007). Ambient noise Rayleigh wave tomography across Europe. *Geophysical Journal International*, 168(1), 259–274. <https://doi.org/10.1111/j.1365-246X.2006.03203.x>
- Yang, Y. T. (2013). An unrecognized major collision of the Okhotomorsk Block with East Asia during the Late Cretaceous, constraints on the plate reorganization of the Northwest Pacific. *Earth-Science Reviews*, 126, 96–115. <https://doi.org/10.1016/j.earscirev.2013.07.010>
- Yao, H., Beghein, C., & Van Der Hilst, R. D. (2008). Surface wave array tomography in SE Tibet from ambient seismic noise and two-station analysis—II. Crustal and upper-mantle structure. *Geophysical Journal International*, 173(1), 205–219. <https://doi.org/10.1111/j.1365-246X.2007.03696.x>
- Yao, H., Gouedard, P., Collins, J. A., McGuire, J. J., & van der Hilst, R. D. (2011). Structure of young East Pacific Rise lithosphere from ambient noise correlation analysis of fundamental-and higher-mode Scholte-Rayleigh waves. *Comptes Rendus Geoscience*, 343(8–9), 571–583. <https://doi.org/10.1016/j.crte.2011.04.004>
- Yao, H., van der Hilst, R. D., & De Hoop, M. V. (2006). Surface-wave array tomography in SE Tibet from ambient seismic noise and two-station analysis—I. Phase velocity maps. *Geophysical Journal International*, 166(2), 732–744. <https://doi.org/10.1111/j.1365-246X.2006.03028.x>
- Yu, S. B., Chen, H. Y., & Kuo, L. C. (1997). Velocity field of GPS stations in the Taiwan area. *Tectonophysics*, 274(1–3), 41–59. [https://doi.org/10.1016/S0040-1951\(96\)00297-1](https://doi.org/10.1016/S0040-1951(96)00297-1)
- Zhan, W. H., Sun, Z. X., Tang, C., Zhu, J. J., & Sun, L. T. (2004). Littoral active fault belt of South China and its control on seismic activity in Taiwan Strait [in Chinese with English abstract]. *Journal of Tropical Oceanography*, 23(4), 19–24.
- Zhao, J. L., Qiu, J. S., Liu, L., & Wang, R. Q. (2015). Geochronological, geochemical and Nd–Hf isotopic constraints on the petrogenesis of Late Cretaceous A-type granites from the southeastern coast of Fujian Province, South China. *Journal of Asian Earth Sciences*, 105, 338–359. <https://doi.org/10.1016/j.jseas.2015.01.022>
- Zheng, H. W., Gao, R., Li, T. D., Li, Q. S., & He, R. Z. (2013). Collisional tectonics between the Eurasian and Philippine Sea plates from tomography evidences in Southeast China. *Tectonophysics*, 606, 14–23. <https://doi.org/10.1016/j.tecto.2013.03.018>
- Zheng, X. F., Yao, Z. X., Liang, J. H., & Zheng, J. (2010). The role played and opportunities provided by IGP DMC of China National Seismic Network in Wenchuan earthquake disaster relief and researches. *Bulletin of the Seismological Society of America*, 100(5B), 2866–2872. <https://doi.org/10.1785/0120090257>
- Zhou, X. M., Sun, T., Shen, W., Shu, L., & Niu, Y. (2006). Petrogenesis of Mesozoic granitoids and volcanic rocks in South China: A response to tectonic evolution. *Episodes*, 29(1), 26.